# DRAG REDUCTION IN CHANNEL FLOW BY TRAVELING WAVE-LIKE SURFACE HEATING/COOLING

**Hiroya Mamori, Koji Fukagata, Shinnosuke Obi**
Department of Mechanical Engineering
Keio University
3-14-1 Hiyoshi, Kohoku-ku, Yokohama 223-8522, Japan,
hiroyamamori@z5.keio.jp

**Jerome Hœpffner**
Institut Jean Le Rond D'Alembert
Universite Pierre et Marie Curie
Tour 55-65, 4 place Jussieu, 75252 Paris Cedex 05,
jerome.hoepffner@upmc.fr

## ABSTRACT

Reduction of skin-friction drag in a channel flow by traveling wave-like surface heating/cooling is investigated by means of linear analysis and direct numerical simulation. The linear analysis reveals that a downstream traveling wave can reduce the skin-friction drag. Due to non-quadrature between the streamwise and the wall-normal velocity disturbances induced by the buoyancy force, non-zero Reynolds shear stress is created in the regions near the walls, which contributes to the skin-friction drag reduction. The direct numerical simulation shows that a traveling wave at a high wavenumber slightly reduces the friction drag in a fully developed turbulent channel flow. The velocity fluctuations and the Reynolds shear stress are slightly attenuated by this control. The friction drag increases for larger magnitudes and lower wavenumbers of the traveling waves. Non-zero mean temperature profile is created due to the turbulent heat flux induced by the control.

## INTRODUCTION

Reduction of the skin-friction drag is of great importance for energy utilization, because the friction drag increases in the turbulent flow and it contributes to e.g., about 50, 90 and 100 % of the total drag in commercial aircrafts, underwater vehicles and pipelines, respectively (Gad-el-Hak, 1994). Since 1990's, different control methods for the skin-friction drag reduction have been proposed, e.g., polymer additives (White and Mungal, 2008), wall oscillations (Karniadakis and Choi, 2003), riblets (Choi et al., 1993) and blowing/suction from the walls (Choi et al., 1994).

Because the quasi-streamwise vortex in the region near the wall exchanges the momentums, the skin-friction drag and the Reynolds shear stress (RSS) increase significantly in wall-bounded turbulent flows. In fact, there is an identity equation relating the RSS and the skin-friction (Fukagata et al., 2002; Bewley and Aamo, 2004). For a fully developed channel flow, the identity equation for the dimensionless friction drag, $D$, reads,

$$D = \underbrace{2}_{D_{lam}} + \underbrace{\frac{3}{2}\mathrm{Re}\int_{-1}^{1}(-y)\left(-\overline{u'v'}\right)dy}_{\Delta D}. \qquad (1)$$

Here, the Reynolds number, $\mathrm{Re} = U_c\delta/\nu$, is defined based on the centerline velocity, $U_c$, and the channel half-width, $\delta$, $-\overline{u'v'}$ is the RSS and $y$ is the wall normal coordinate extending from $y = -1$ (lower wall) to $y = 1$ (upper wall). This equation indicates that the skin-friction drag is divided into the laminar contribution, $D_{lam} = 2$, and the drag increment, $\Delta D$, which is the integration of the $y$-weighted RSS. Friction drag below the laminar level is achieved if $\Delta D < 0$.

Based on the implication of this identity equation, Min et al. (2006) proposed a new predetermined control method, by which large drag reduction effect can be achieved without using any sensors. In their method, the local blowing/suction velocity from the walls, $v_w$, is given as

$$v_w = a\cos\left(k(x - ct)\right), \qquad (2)$$

where $x$ and $t$ denote the streamwise coordinate and the time, respectively. The parameters, $a$, $k$ and $c$, represent the amplitude, the wavenumber and the wavespeed of the traveling wave. Min et al. (2006) predicted the amount of drag reduction by coupling the linear analysis and Eq. (1), as shown in Fig. 1. The friction drag was reduced ($\Delta D < 0$) by upstream traveling waves ($c < 0$) and in such cases negative RSS (if the RSS in ordinary turbulent channel flows is called positive) is created in the regions near the walls. Min et al. (2006) also confirmed the drag reduction effect in

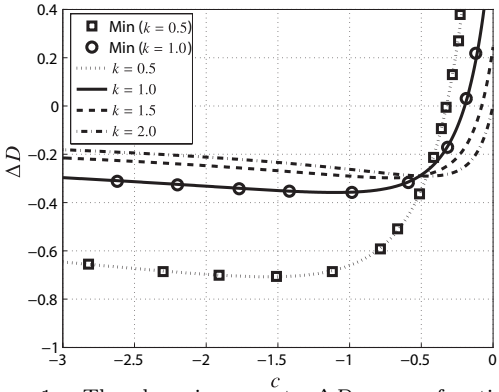


Figure 1: The drag increment, $\Delta D$, as a function of wavenumber, $c$ by the traveling wave-likes surface blowing/suction control of Min et al. (2006) reproduced by Mamori et al. (2008). The Reynolds number is $\mathrm{Re} = 2000$ and the waveamplitude of the traveling wave is $a = 0.1$.

a fully developed turbulent channel flow by means of direct numerical simulation (DNS).

Although the traveling wave-like surface blowing/suction of Min et al. (2006) is an effective control for the drag reduction, it is difficult to fabricate such a blowing/suction device in practice. As an alternative, we propose here a similar control method using a traveling wave-like heating/cooling of the walls. With this method, the buoyancy force is expected to induce the fluid motion like blowing/suction in the region near the wall. The traveling wave-like heating/cooling device requires stripped heaters and coolers, which can be fabricated more easily than the blowing/suction device. As a drag reduction technique using the buoyancy force, Yoon et al. (2006) proposed the periodically arrayed heating/cooling in a fully developed channel flow which produces similar effects to the spanwise wall oscillations. They could achieved 35% drag reduction by an optimum strip size of heating/cooling array.

The objective of the present study is to investigate the possibility of skin-friction drag reduction by the above-mentioned traveling wave-like surface heating/cooling. Linear analysis and direct numerical simulation are used to compute the velocity fields in a laminar flow and a fully developed turbulent flow, respectively, and the drag is computed by using the identity equation (1). Effects of wavenumber, wavespeed, and amplitude of the traveling wave are also investigated.

## LINEAR ANALYSIS

### Solution Techniques

A two-dimensional channel flow is considered. The governing equations are the two-dimensional and incompressible continuity, Navier-Stokes and energy equations. Figure 2 shows the flow geometry, the coordinate systems and the control input. All the quantities are made dimensionless by using the centerline velocity, $U_c$, the channel half-height, $\delta$, and the temperature amplitude of the traveling wave, $\Delta T$. The velocity components in the $x^*$ (streamwise) and $y^*$ (wall-normal) directions are denoted as $u$ and $v$, respectively. The pressure and the temperature are denoted as $p$ and $T$, respectively. The asterisk denotes the position on the fixed coordinates. The base flow, $U$, is set to be the laminar Poiseuille profile, i.e., $U = 1 - y^{*2}$.

The periodic boundary condition is employed in the streamwise direction and the no-slip condition is employed at the walls. As a control input, the wall temperature is given as a traveling wave-like surface heating/cooling, which reads,

$$T_{w\pm} = \mp \cos\left(k^*\left(x^* - ct^*\right)\right), \tag{3}$$

where $T_{w+}$ and $T_{w-}$ are the wall temperatures at the upper and the lower walls, respectively. Hereafter, the temperature is made dimensionless by using the temperature amplitude of control input, $\Delta T$.

The problem can be reduced into a steady problem by introducing a coordinate transformation from the fixed coordinates to the coordinates traveling with the wave i.e., $x := x^* - ct^*, y := y^*, t := t^*$ (Javanovic et al., 2006). The unsteady term of incompressible Navier-Stokes equation on the fixed coordinates reads

$$\frac{\partial}{\partial t^*} = \frac{\partial}{\partial t} - c\frac{\partial}{\partial x}. \tag{4}$$

Because the system can be assumed steady in this moving coordinates, the first term in the right hand side of Eq. (4) is eliminated. The boundary condition (Eqs. (3)) in the moving coordinates reads

$$T_{w\pm} = \mp \cos\left(kx\right). \tag{5}$$

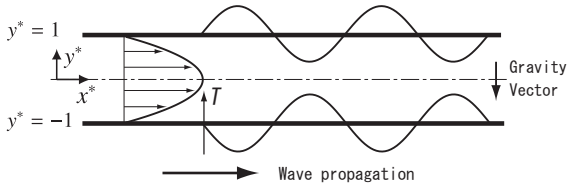


Figure 2: Flow geometry, coordinate system and the traveling wave-like surface heating/cooling as the control input.

The governing equations are linearized: $u = U + u'$, $v = v'$, $p = P + p'$ and $T = T'$ are substituted into the governing equations and the higher order terms of disturbances are neglected. Here, $U$ and $P$ denote the velocity and pressure of the base flow, respectively, and the prime denotes the disturbance component. The linearized disturbance equations are expressed as

$$\frac{\partial u'}{\partial x} + \frac{\partial v'}{\partial y} = 0, \tag{6}$$

$$-c\frac{\partial u'}{\partial x} + U\frac{\partial u'}{\partial x} + v'\frac{\partial U}{\partial y} = -\frac{\partial p'}{\partial x} + \frac{1}{\mathrm{Re}}\nabla^2 u', \tag{7}$$

$$-c\frac{\partial v'}{\partial x} + U\frac{\partial v'}{\partial x} = -\frac{\partial p'}{\partial y} + \frac{1}{\mathrm{Re}}\nabla^2 v' + \mathrm{Ri}T', \tag{8}$$

$$-c\frac{\partial T'}{\partial x} + U\frac{\partial T'}{\partial x} = \frac{1}{\mathrm{Re}\cdot\mathrm{Pr}}\nabla^2 T'. \tag{9}$$

Here, Re, Pr and Ri are the Reynolds, Prandtl and Richardson numbers, respectively. The third term of the right hand side in Eq. (8) is the buoyancy force term which is incorporated by using the Boussinesq approximation. The temperature is assumed to be a passive scalar so that Eq. (9) can be solved independently.

Due to the periodic condition in the streamwise direction, the Fourier transformation can be applied for $f = (u, v, p, T)^T$ as

$$f' = \mathrm{Real}\left(\hat{f}(y)\exp(ikx)\right), \tag{10}$$

where the hat denotes the Fourier coefficient. In the wall-normal direction, the Fourier coefficients are discretized by using the Chebyshev collocation points method and the Chebyshev differential matrix of a MATLAB function (Weidman and Reddy, 2000), is applied for the $y$-derivative operators. The node number is set to $N = 128$, which was found to be sufficient in terms of node dependency. As a result of these transformations, Eq. (9) is expressed as a system matrix equation for the discretazed temperature, $\hat{\mathbf{T}}$,

$$\mathbf{A_1}\hat{\mathbf{T}} = \mathbf{b_1}, \tag{11}$$

where, $\mathbf{A}_1$ is the system matrix, $\mathbf{b_1}$ is the vector including the temperature boundary condition. The solution to this matrix equation is easily obtained by $\hat{\mathbf{T}} = \mathbf{A}_1^{-1}\mathbf{b}_1$ and the spatial distributions of $T'$ is computed by applying the inverse Fourier transform to the solution. The distribution of the buoyancy force is obtained by the substituting temperature distribution to the buoyancy force term in Eq. (8).

Because Eqs. (6)-(8) are also linearized, the Fourier transformed system is expressed as a matrix equation,

$$\mathbf{A}\hat{\mathbf{q}} = \mathbf{b}, \tag{12}$$

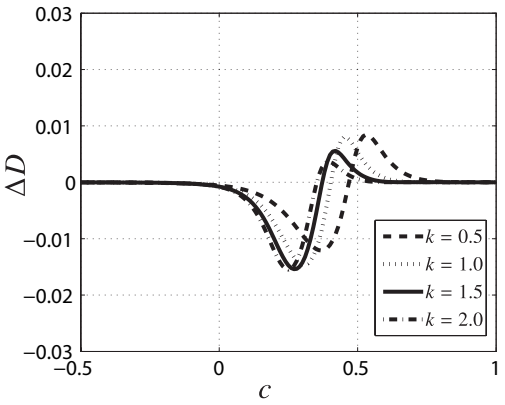


Figure 3: The drag increment, $\Delta D$, as a function of wavenumber, $c$, at Re = 2000 and Ri = 0.0945.

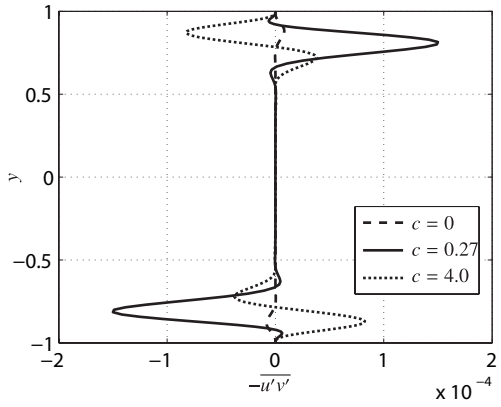


Figure 4: Profile of the Reynolds shear stress at $k = 1.5$, Re = 2000 and Ri = 0.0945.

where $\mathbf{A}$ is the system matrix, $\hat{\mathbf{q}} = (\hat{\mathbf{u}}, \hat{\mathbf{v}}, \hat{\mathbf{p}})$ is the discretized Fourier coefficient vector of the velocity, pressure and $\mathbf{b}$ is the vector including the Fourier transformed buoyancy force distribution.

The solution to this matrix equation is similarly obtained by $\hat{\mathbf{q}} = \mathbf{A}^{-1}\mathbf{b}$ and the spatial distributions of $u'$, $v'$ and $p'$, are computed by the inversed Fourier transform to the solution. Finally, $\Delta D$ is computed by using Eq. (1). With this method, we can predict the drag increment (which is essentially the nonlinear effect) from the linear solution.

#### Results and discussion

The control effect is evaluated by the computed drag increment, $\Delta D$. The nondimensional numbers are set at Re = 2000, Pr = 0.71 (air) and Ri = 0.0945, which correspond to the temperature amplitude of the traveling wave at 3 K in a channel flow with $\delta = 10$ cm and $U_c = 0.3$ m/s.

Figure 3 shows $\Delta D$ as a function of the wavespeed, $c$. This figure indicates that at $k = 1.5$ the drag reduces for $-0.2 < c < 0.37$ and increases for $0.37 < c < 0.6$. The drag is nearly unchanged in the ranges of $c < -0.2$ and $c > 0.6$. Unlike the blowing/suction control by Min et al. (2006), the drag reduction is achieved with the downstream traveling wave in the case of wall heating/cooling.

Figure 4 shows the RSS distributions for $k = 1.5$ under different wavespeeds, $c = 0$, 0.27, and 0.4. For the downstream traveling wave at $c = 0.27$, where the maximum drag reduction is obtained, it is clearly observed that negative (positive) Reynolds shear stress is produced in the region near the lower (upper) wall; whereas for the maximum drag increasing case, at $c = 0.4$, the Reynolds shear stress are positive and negative in the regions near the lower and upper walls, respectively. For the standing wave, $c = 0$, the Reynolds shear stress takes slightly negative and positive value in the same region.

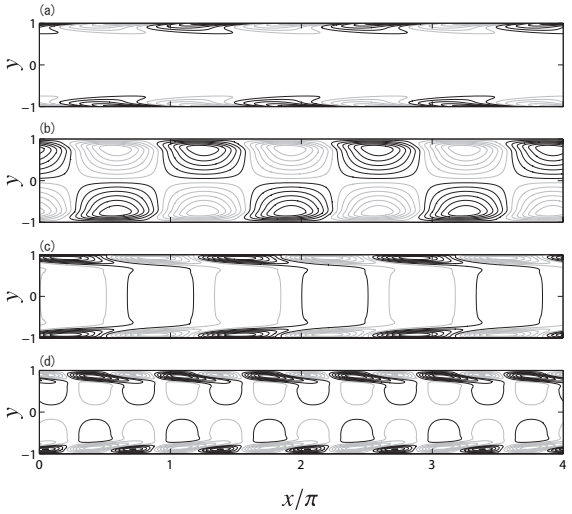


Figure 5: Contour plots of disturbance components by the traveling wave for $c = 0.27$ and $k = 1.5$; (a) $T'$, (b) $v'$, (c) $u'$ and (d) $-u'v'$. The line increments are 0.15, 0.001, 0.005 and 0.00002 for $T'$, $v'$, $u'$ and $-u'v'$, respectively. The black is the positive value and gray is the negative value.

Figures 5 show the disturbance fields at $c = 0.27$ and $k = 1.5$ which produced the maximum drag reduction. The buoyancy force is induced by temperature disturbance ($T'$) as shown in Fig. 5(a), due to the heating/cooling applied to the walls. Accordingly, as shown in Fig. 5(b), the positive and negative wall-normal velocities ($v'$) are induced in the regions of positive and negative $T'$, respectively. Figure 5(c) shows that the streamwise velocity ($u'$) is generated as the response of the system. Due to the subtle phase lead of $u'$ near the walls, $u'$ and $v'$ become non-quadrature and non-zero values of $-\overline{u'v'}$ are created in the regions near the walls, as shown in Fig. 5(d). This $-u'v'$ is asymmetric: negative (positive) values appear more frequently near the lower (upper) wall and this contributes to the Reynolds shear stress distribution as observed in Fig. 4.

## DIRECT NUMERICAL SIMULATION

The drag reduction effect by the present control in a fully-developed channel flow is investigated by means of direct numerical simulation (DNS). The DNS code is based on the channel flow code by Fukagata et al. (2006), which is originally developed for the pipe flow (Fukagata and Kasagi, 2002). The governing equations are incompressible and three dimensional continuity, Navier-Stokes and energy equations. For a spatial discretization, the energy conservative second-order finite difference method for the advection term and the second-order central differential method for the viscosity term are employed. The temporal integration is done by using the low-storage third order Runge-Kutta/Crank-Nicolson (RK3/CN) scheme. A velocity and pressure are

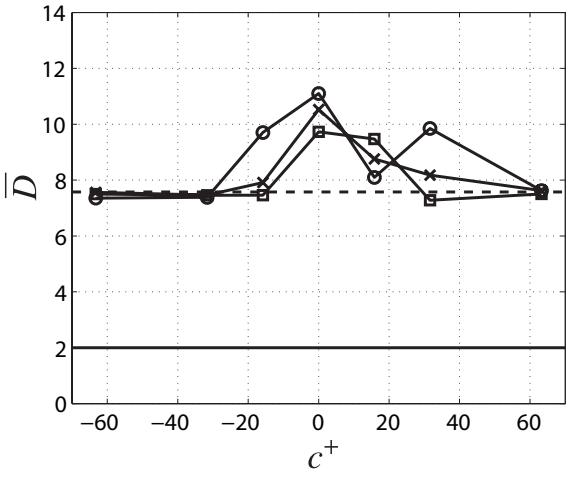


Figure 6: Time-averaged skin-friction drag, $\overline{D}$, as a function of wavenumber, $c^+$, in turbulent channel flow at Ri = 0.2: $-\circ-$, $k = 0.5$; $-\times-$, $k = 1.0$; $-\square-$, $k = 1.5$; broken line, uncontrolled level; solid line, laminar level.

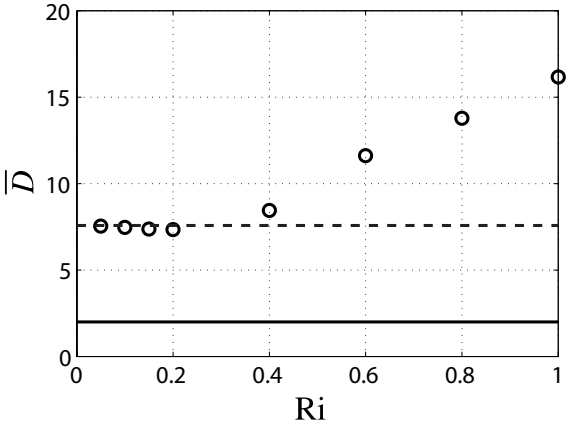


Figure 7: Time-averaged skin-friction drag, $\overline{D}$, as a function of the Richardson number, Ri, at the fixed wavenumber and wavespeed, $k = 1.5$ and $c^+ \approx 32$, respectively. Broken line, uncontrolled level; solid line, laminar level.

coupled by delta-form fractional step method. The fast Fourier transform (FFT) in the streamwise and the spanwise directions and the tridiagonal matrix in wall-normal direction are used to solve the pressure Poisson equation. The flow domain is set to be $L_x \times L_y \times L_z = 4\pi\delta \times 2\delta \times 3.5\delta$ and the number of grids are $N_x \times N_y \times N_z = 256 \times 96 \times 128$. The mass flow rate is kept constant. All simulations is started from a velocity field of an uncontrolled fully developed channel flow. The Reynolds number is Re = 4200 based on the channel half-height and the laminar centerline velocity, which corresponds to $\mathrm{Re}_\tau \approx 180$ based on the friction velocity, $u_\tau$, of the uncontrolled flow. The boundary condition used is the same as that used for the linear analysis in the previous section.

Figure 6 shows the time-averaged friction drag, $\overline{D}$, as a function of the wavespeed, $c^+$, for the different wavenumbers, $k$. The superscript of + denotes the wall unit of the uncontrolled flow. The Richardson number is fixed at Ri = 0.2. The friction drag is found to increase for the cases of $c^+ \approx 0$. For faster wave (i.e., the cases of larger $|c|$), the friction drag takes similar values to that of the uncontrolled flow. In any cases, significant drag reduction like the control by blowing/suction of Min et al. (2006) or that of heating/cooling in laminar flows (presented in the previous section) is not observed. Only small amount of drag reduction is observed at $c^+ \approx 32$ and $k = 1.5$. In the followings, we focus on the flow field of this case.

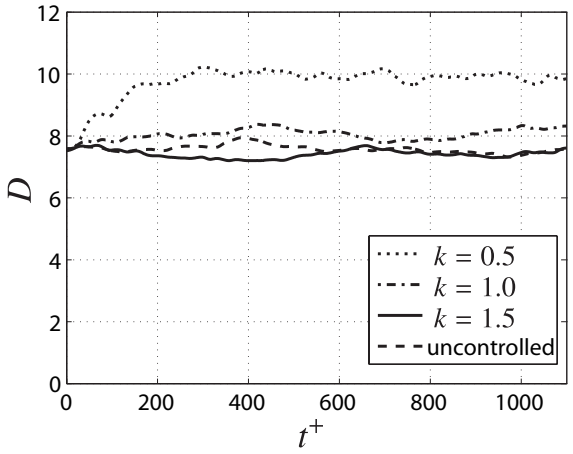


Figure 8: Time history of the skin-friction drag, $D$, by the different wavenumber compared with the uncontrolled flow.

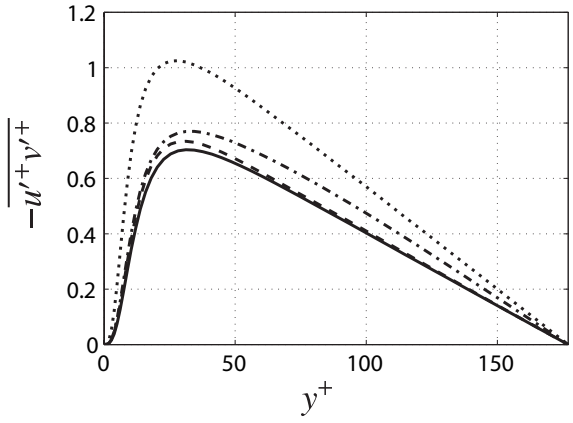


Figure 9: Profile of the Reynolds shear stress. The lines are the same as Fig. 8.

Figure 7 shows the time-averaged friction drag as a function of the Richardson number, Ri, at $k = 1.5$ and $c^+ \approx 32$. The friction drag is slightly reduced at Ri = 0.2. However, for Ri $> 0.4$, $\overline{D}$ is found to be nearly proportional to the Richardson number. It is indicated that the strong buoyancy force increases the friction drag, but a relatively weak buoyancy force can induce slight drag reduction.

Figure 8 shows the time history of the friction drag in the cases of $k = 0.5$ $(\lambda^+ \approx 2200)$, $k = 1.0$ $(\lambda^+ \approx 1100)$ and $k = 1.5$ $(\lambda^+ \approx 740)$ , and the uncontrolled flow. Here, $\lambda^+$ is the wavelength of the traveling wave in the wall unit and $t = 0$ denotes the time instance when the control begins. The Richardson number and the wavespeed are fixed at Ri = 0.2 and $c^+ \approx 32$, respectively. Slight drag reduction ($\approx -3.1\%$) is obtained at $k = 1.5$. As the wavenumber is decreased, the drag is increased, i.e., 5.7% for $k = 1.0$ and 31% at $k = 0.5$.

The turbulence statistics is computed by averaging over the homogeneous direction as well as in time after the flow reaches the steady state. The temporal average is taken in the period of $t^+ \approx 1100 - 2200$.

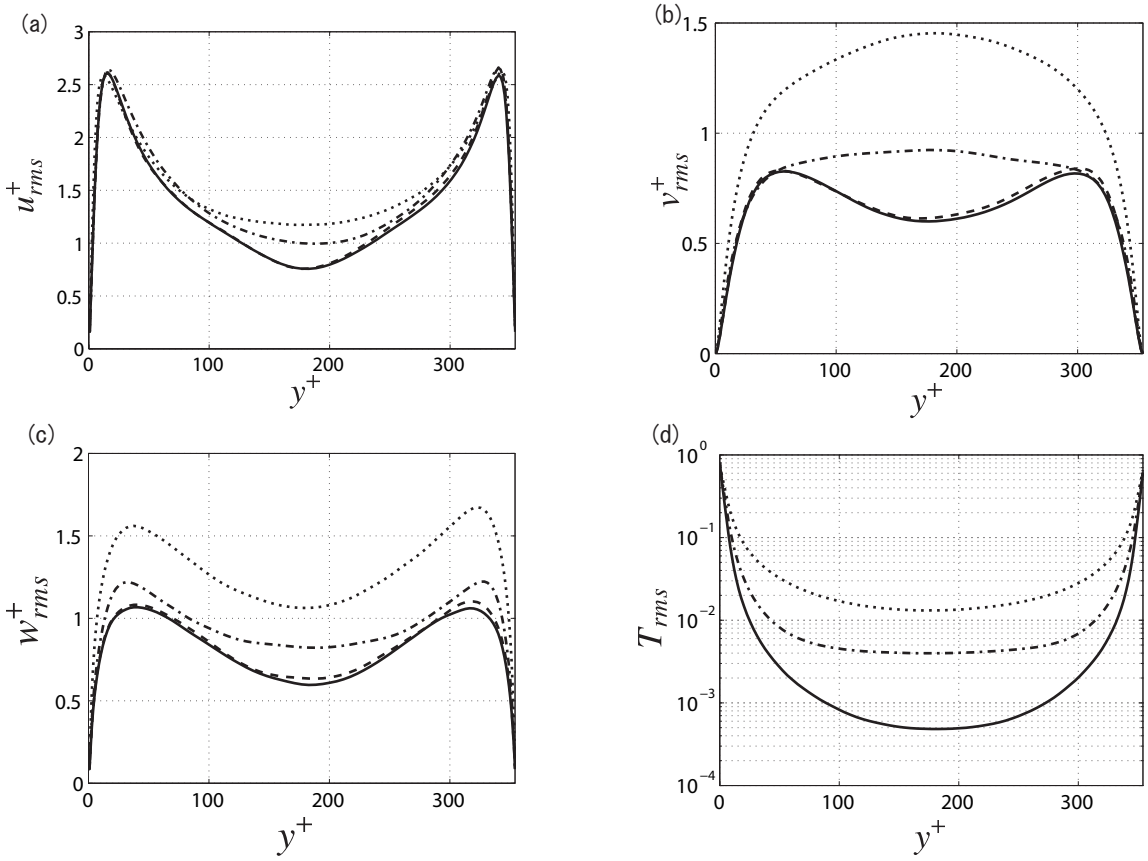


Figure 10: Profiles of the root-mean-square components at $c^+ \approx 31$ and Ri = 0.2; (a) streamwise velocity, (b) wall-normal velocity, (c) spanwise velocity, (d) temperature. The lines are the same as Fig. 8.

The RSS profiles for different wavenumbers are shown in Fig. 9. It is observed that the RSS decreases as increasing the wavenumber. The peak of the RSS at $k = 1.5$ is slightly smaller than that of the uncontrolled flow. According to Eq. (1), the skin-friction drag is the $y$-weighted integration of the RSS: the slight drag reduction observed above is due to the reduced RSS in the region near the wall.

Figures 10 show the root-mean-square (rms) of the velocity components and the temperature for different wavenumbers. As shown in Fig. 10(a), the rms streamwise velocity for $k = 1.5$ almost collapses with that of the uncontrolled flow. For the cases other than $k = 1.5$, it increases in the channel center region as decreasing the wavenumber. Figures 10(b) and (c) reveal that the rms wall-normal and spanwise velocities for the case of $k = 1.5$ are slightly reduced as compared to those of the uncontrolled flow, which indicates that the cross-sectional motion (such as that by the quasi-streamwise vortex) is slightly suppressed by the control input. It is also observed in Figs. 10(b) and (c) that higher wavenumber causes increase of the rms wall-normal and spanwise velocities throughout the channel. Figure 10(d) shows the rms temperature profiles. Stronger fluctuations are observed for higher wavenumbers. This is consistent with the trend in the wall-normal velocity fluctuations, which is additionally generated by the buoyancy force. Due to the system response, the rms spanwise velocity also increases. Although the rms temperature of $k = 1.5$ case is almost unchanged from that of the uncontrolled flow, the buoyancy force seemingly works to slightly suppress the velocity fluctuations.

Figure 11 shows the mean temperature profiles for different control wavenumbers. Due the symmetric control input and the gravitational force, the mean temperature becomes antisymmetric. For instance, for the case of $k = 0.5$, it is negative in the region near the wall at $0 < y^+ < 28$ and positive at $y^+ > 28$ in the lower half of channel. The peak of the temperature in the region near the wall decreases as increasing the wavenumber. In fact, there is a equation between mean temperature and $-\overline{v'T'}$ (Fukagata et al, 2005) which reads,

$$\overline{T} = \frac{\mathrm{Nu}}{4\mathrm{PrRe}} - \int_{-1}^{y} \left(-\overline{v'T'}\right) dy, \tag{13}$$

here Nu is a Nusselt number. This identity equation suggests that the decreased temperature is due to the decreased turbulent heat flux, $-\overline{v'T'}$ shown in Fig. 12.

## CONCLUSIONS

Skin-friction drag reduction by the traveling wave-like surface heating/cooling in the channel flow is investigated numerically.

For the laminar flow, the linear analysis suggests that significant amount of drag reduction can be achieved by downstream traveling waves. The buoyancy force induced by the surface heating/cooling generates the non-quadrature between the disturbance velocity components, resulting in the skin-friction drag reduction.

For the fully developed turbulent channel flow, direct numerical simulation reveals that slight drag reduction can be obtained by downstream traveling waves. The friction drag, however, increases from the uncontrolled flow for lower

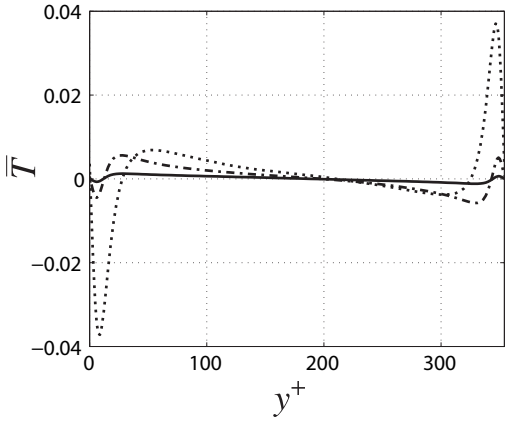


Figure 11: The profile of the mean temperature at $c^+ \approx 32$. The lines are the same as Fig. 8.

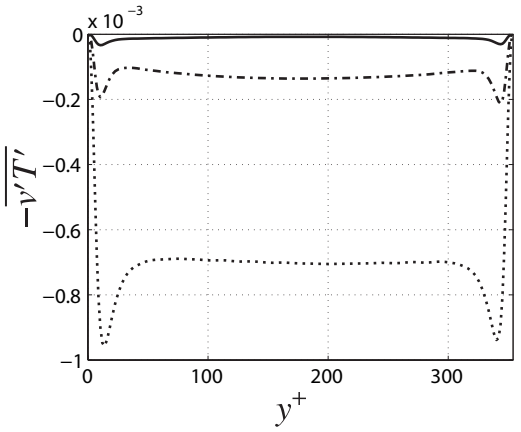


Figure 12: The profile of turbulent heat flux, $-\overline{v'T'}$. The lines are the same as Fig. 8.

wavenumbers and stronger buoyancy forces. The control input with larger wavenumber generates the larger temperature fluctuations; the later temperature fluctuations create the velocity fluctuations due to the buoyancy force term. It is also found that the turbulent heat flux can create non-zero profile of the mean temperature despite the essentially symmetric spatial distribution of the control input.

## ACKNOWLEDGMENTS

The authors are grateful to Drs. Nobuhide Kasagi and Yosuke Hasegawa (The University of Tokyo) and Dr. Kaoru Iwamoto (Tokyo University of Agriculture and Technology) for fruitful discussions. This work was supported through Grant-in-Aid for Scientific Research (A) (No. 20246036) by Japan Society for the Promotion of Science (JSPS), Grant-in-Aid for JSPS Fellows (No. 19-07821), and Keio Gijuku Academic Funds.

## REFERENCES

Bewley, T. R., and Aamo, O. M., 2004, "A win-win mechanism for long-drag transients in controlled two-dimensional channel flow and its implication for sustained drag reduction", *J. Fluid Mech.*, Vol. 499, pp. 183-196.

Choi, H., Moin, P., and Kim, J., 1993, "Direct numerical simulation of turbulent over the riblets", *J. Fluid Mech.*, Vol. 255, pp. 503-539.

Choi, H., Moin, P., and Kim, J., 1994, "Active turbulence control for drag reduction wall-bounded flows", *J. Fluid Mech.*, Vol. 262, pp. 75-110.

Fukagata, K., Iwamoto, K., and Kasagi, N., 2002, "Contribution of Reynolds stress distribution to the skin friction in wallbounded flows", *Phys. Fluids*, Vol. 14, pp. L73-L76.

Fukagata, K., and Kasagi, N., 2002, "Highly energy-conservative finite difference method for the cylindrical coordinate system", *J. Comput. Phys.*, Vol. 181, pp. 478-498.

Fukagata, K., Iwamoto, K., and Kasagi, N., 2005, "Novel turbulence control strategy for simultaneously achieving friction drag reduction and heat transfer augmentation", *Proc. 4th Symp. Turbulence and Shear Flow Phenomena*, pp. 307-312.

Fukagata, K., Kasagi, N., and Koumoutsakos, P., 2006, "A theoretical prediction of friction drag reduction in turbulent flow by superhydrophobic surfaces", *Phys. Fluids*, Vol. 18, pp. 051703.

Gad-el-Hak, M., 1994, "Interactive control of turbulent boundary layers: A futuristic overview", *AIAA J.*, Vol. 32, pp. 1753-1765.

Javanovic, M. R., Moarref, R., and You, D., 2006, " Turbulence suppression in channel flows by means of a streamwise traveling wave", *Center for Turbulence Research Proceeding of the Summer Program 2006*, pp. 481-494.

Karniadakis, G. E., and Choi, K., 2003, "Mechanism on transverse motion in turbulent wall flow", *Annu. Rev. Fluid Mech.*, Vol. 35, p. 45-62.

Mamori, H., Fukagata, K., Hœpffner, J., and Obi, S., 2008, "Linear analysis of drag reduction in channel flow by wall heating/cooling", *Proc. 7th EUROMECH Fluid Mech. Conf.*, Manchester, UK, p. 207.

Min, T., Kang, S. M., Speyer, J. L., and Kim, J., 2006, "Sustained sub-laminar drag in a fully developed channel flow", *J. Fluid Mech.*, Vol. 558, pp. 309-318.

Weidman, J. A. C., and Reddy, S. C., 2000, "A MATLAB Differentiation Matrix Suite", *ACM Trans. Math. Software*, Vol. 26, pp. 465-519.

White, C. M., and Mungal, M. G., 2008, "Mechanics and Prediction of Turbulent Drag Reduction with Polymer Additives", *Annu. Rev. Fluid Mech.*, Vol. 40, pp. 235-256.

Yoon, H. S., El-Samni, O. A., and Chun, H. H., 2006, "Drag reduction in turbulent channel flow with periodically arrayed heating and cooling strips", *Phys. Fluids*, Vol. 18, pp. 025104.